CFD modelling of the air preheater fired with gas mixture to find the cause of the preheater damage

Tomasz Sobota*, *Dawid* Taler, *Mariusz* Granda, and *Magdalena* Szymkiewicz

Cracow University of Technology, Department of Thermal Processes, Air Protection and Waste Utilisation, ul. Warszawska 24, 31-155 Cracow, Poland

Abstract. Since various fuels, such as natural gas, blast furnace gas, coke oven gas, and a mixture of the three, are burned in the boiler, there is a danger of corrosion caused by sulphuric acid. Sulphur dioxide produced after combustion and condensed water vapour from flue gases on cold tube surfaces form sulphuric acid. Sulphuric acid solution flowing down the vertical tubes of the air heater causes corrosion not only of the air heater tubes but also of the horizontal water heater tubes located below. A simulation of the flow and heat exchange on the flue gas and air sides was performed to determine the areas of the air heater where the temperature of the air heater tubes is low and condensation may occur. Based on the measured air and flue gas mass flows, the measured flue gas temperatures behind the heater, and the air temperature at its inlet, the flue gas temperature before the air heater was determined using the ε-NTU (Effectiveness-Number of Transfer Units) method. Based on CFD modelling and experimental research, the areas in the heater where sulphuric acid can form at given outside air temperatures were determined.

1 Introduction

In power boilers, the chemical energy of the fuel burned is converted into thermal energy to produce a working medium in the form of high-temperature and high-pressure steam, which is then used to drive the turbine and produce electricity or to supply the plant with heat and electricity. Energy resources such as coal, oil, natural gas, or process gas fuels such as blast furnace or coke oven gas can be used as fuel. Heating surfaces like evaporators, boiler drums, steam superheaters, boiler feed water heaters (economizers) and air heaters are the main elements of the power boiler. Failure of the boiler's heating surfaces may lead to the boiler shutdown and, thus, to a power plant stop. The cause of the failure may be related to water-side corrosion, fire corrosion, exceeding the permissible temperature of the piping material, stress or erosion. The greatest number of failures is associated with damage to boiler evaporator tubes, followed by damage to elements of live and reheated steam superheaters and the economizer. The main causes of corrosion damage to boiler heating

* Corresponding author: tomasz.sobota@pk.edu.pl

surfaces are divided into high-temperature corrosion, corrosion caused by molten salts, and sulphuric acid dew point corrosion.

High-temperature corrosion most often occurs on power boiler tubes [1]. This type of corrosion is strongly associated with the presence of sodium (Na) and vanadium (V) in the fuel. Molten salt corrosion occurs in waste incineration boilers and is caused by chlorine (Cl) present in the molten salt. It results in the corrosion of the power boiler evaporator and platen superheater [2]. Sulphuric acid dew point corrosion belongs to the group of so-called low-temperature corrosion. Burned in power and utility boilers, fossil fuels such as coal, petroleum derivatives or process gases (coke oven and blast furnace) contain a certain amount of sulphur. During the combustion process, present in the fuel, sulphur is combined with oxygen to form sulphur dioxide (SO_2) in the partial oxidation process and sulphur trioxide (SO_3) in the full oxidation process [3]. Most of the recent boiler tube corrosion has been observed under boiler operation with more aggressive environments than before. Therefore, the failure analysis performs a very important role in clarifying the cause of boiler tube corrosion in the actual boiler.

Kumar et al. investigated sources of damaged tubes in power boilers [4]. Visual inspection, strength measurement together with determination of chemical composition and metallography were applied. The tubes' damage resulted from complex creep, corrosion and erosion mechanisms. Thermal waste incineration plants, in particular, are at high risk of corrosion due to the fuel's high chlorine content. Marx et al. developed an online corrosion sensor to monitor corrosion in incineration plants [5]. The sensor enables corrosion detection semi-quantitatively and with variable time resolution.

Cross-flow tubular heat exchangers are widely used in many applications, including power boilers, heating and ventilation, and car radiators. A simplified method can be used to design and perform heat exchanger calculations, like ε-NTU (effectiveness – Number of Transfer Units). Węglarz et al. presented a method for determining steam and flue gas temperatures at the outlet of a two-pass co-current steam superheater [6]. Yin and Zhou analysed sources of reheater tubes overheating in supercritical power boilers [7]. They proposed a multistep prediction model of reheater tube calculation. Modliński et al. developed a mathematical procedure for reheater metal temperature determination [8], which combines CFD calculation flue gas temperature and a one-dimensional mathematical model of steam flow in a reheater. Chantasirivan investigated the optimal location of the heat exchange devices (economizer, air heater, flue, gas dryer) in the utility boiler to reduce flue gas temperature and increase boiler efficiency [9]. Numerical models of steam generator and heat recovery devices were developed to calculate flue gas temperature distribution in steam generator second pass.

2 Boiler operation

The boiler is a part of the power unit used in the foundry for electricity generation and supplying the municipal district heating network with hot water. The boiler (Figure 1) is a three-pass boiler with natural water circulation. The nominal operating parameters of the boiler are as follows: steam capacity 41.667 kg/s, temperature and pressure of superheated steam 540.5°C and 9.17 MPa, respectively. The power boiler main steam temperature is controlled by two spray attemperator systems that are located at the inlet to the superheaters SH2 and SH3 (Figure 1).

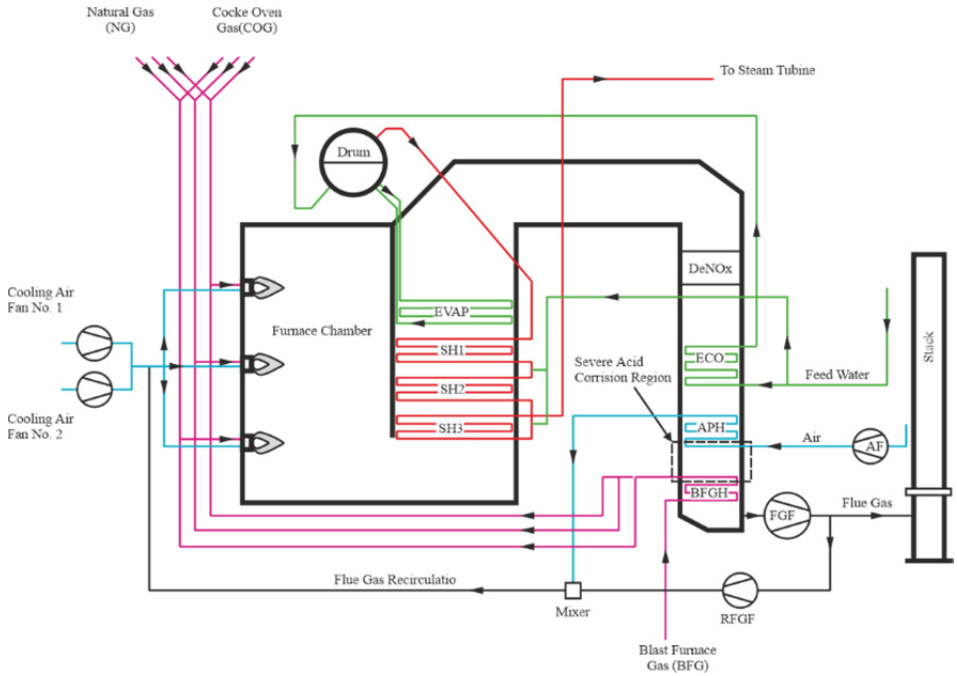

Fig. 1. Schematic diagram of boiler and location of failure; EVAP – boiler evaporator, ECO – feed water heater, APH – air preheater, SH1, SH2, SH3 – first, second and third stage of main steam superheater respectively, BFGH – blast furnace gas heater, AF – forced draft air fan, FGF – induced draft flue gas fan, RFGF – gas recirculation fan.

The boiler is designed to burn the fuel, which is a mixture of the blast furnace (BFG), natural (NG) and coke oven (COG) with different proportions, blast furnace gas alone or natural gas alone. The boiler can operate in the full load range, burning blast furnace gas alone or natural gas alone. However, it is not designed to burn only coke oven gas, the maximum amount of which covers about 30% of the maximum load. The blast furnace and coke oven gases used in the combustion process contain sulphur and its compounds in an allowed amount.

In the third draft of the boiler, a feed water heater, a tubular air preheater and a blast furnace gas heater are installed. Above the economiser, space is provided for the installation of a flue gas denitrification system. The air heater (APH) is a two-pass heat exchanger with a vertical, smooth tube system in a staggered arrangement. Flue gases flow inside the heat exchanger tubes and air from outside. The ambient air is fed directly to the exchanger. An important issue is the manner of the air supply - a duct with a circular cross-section does not run straight, and immediately before the inlet to the air heater, it expands suddenly, changing the cross-section from circular to rectangular.

A heat exchanger BFGH, which works in a blast furnace gas (BFG) heating system is placed beneath the air preheater. The blast furnace gas heating system consists of two heat exchangers - one built in the third draft receives heat from the flue gas and the other in the BFG gas inlet channel. The system increases boiler efficiency by lowering the temperature of flue gases when blast furnace gas (BFG) is burnt. The BFG heat exchanger is made of spiral fin tubes. Both air and blast furnace gas heaters are made of carbon steel.

After a certain period of boiler operation, alarming symptoms appeared. One of these was the impossibility of a boiler to achieve maximum continuous output when burning blast furnace gas. The pressure in the combustion chamber increased due to a lack of draft. The inspection carried out after the boiler had been shut down showed that the lower tube

sheet of the air preheater from the air inlet side had been significantly corroded. The spaces between the fins of the BFG heater tubes were also blocked.

Despite the termination of blast furnace gas combustion, corrosion continued, increasing the degree of damage to the air heater and destroying (perforating) the blast furnace gas heater from the external air supply side.

3 Thermal calculation of the air heater

The effect of progressive corrosion of the air heater and the blast furnace gas heater was to shut down the boiler. To determine the causes of air heater corrosion and damage to blast furnace gas heater tube, thermal modelling of the air heater using the e-NTU method and thermal-flow modelling using CFD software was carried out. The analysed air heater is a two-pass heat exchanger with a cross-flow of non-mixing working media (Figure 2). Exhaust gases from the boiler flow inside the tubes while the air washes from outside.

The purpose of the air heater thermal modelling was to determine the temperature of working mediums at characteristic points of the exchanger: for air at the end of the first gear and at the exchanger outlet, and for flue gases - at the exchanger inlet and at the middle of its height. The ambient air temperature and exhaust gases behind the air heater were known from measurements.

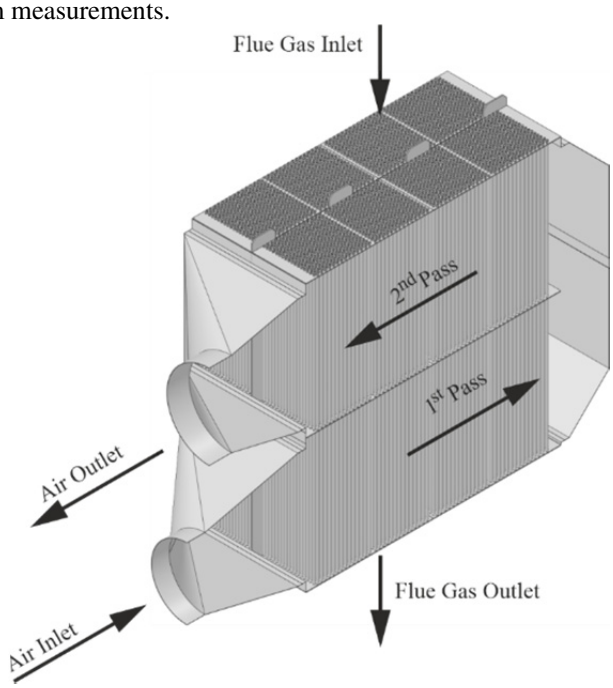

Fig. 2. Air heater (a two-pass heat exchanger with a cross-flow of non-mixing working media). The basic geometrical dimensions of the tubular air heater are material - P235GH-TC1 (carbon steel), tube type - smooth, tube arrangement - staggered, tube length - 3 m, number of tubes L = 8092, total heat transfer area 5872.43 m^2.

On the basis of the knowledge of the chemical composition of blast furnace, coke oven and natural gas gases and their shares in the fuel burned (Table 1), the chemical composition of seven mixtures of fuel burned in the boiler was determined. These data were then used to calculate the theoretical air demand, the volume flow rate and the volume flow rate of the flue gas resulting from the combustion of each combustible gas mixture - Table 2.

Table 1. Chemical composition of combusted gases (a) and its volumetric flow rates in the fuel (b).

a)

	Composition, % mol/mol									
	H_2	CO_2	CH_2	C_2H_6	O_2	N_2	CO	CH_4	C_3H_8	C_3H_6
Coke Oven Gas (COG)	46.7	1.7	1.5	1.6	0.2	5.8	4.7	37.0	0.08	0.13
Blast Furnace Gas (BFG)	3.5	20.4	–	–	0.58	53.1	22.4	0.05	–	–
Natural Gas (NG)	–	0.2	–	1.0	–	1.0	–	97.8	–	–

b)

Gas volumetric flow rates in the combusted fuel, nm^3/h							
	Mix 1	Mix 2	Mix 3	Mix 4	Mix 5	Mix 6	Mix 7
Coke Oven Gas (COG)	1480	1502	1505	3145	–	–	–
Blast Furnace Gas (BFG)	75665	75364	79400	85964	82470	112227	–
Natural Gas (NG)	3181	1543	586	–	–	–	10931

Table 2. Calculated theoretical air demand, excess air coeff., air and flue gas volumetric flow rates.

	Mix 1	**Mix 2**	**Mix 3**	**Mix 4**	**Mix 5**	**Mix 6**	**Mix 7**
Theoretical air demand P_t, m^3_{pow}/m^3	1.030	0.856	0.742	0.755	0.594	0.594	9.477
Excess air coefficient λ	1.218	1.193	1.347	1.208	1.432	1.460	1.264
Air volumetric flow rate V_p, Nm^3/h	100791	80156	81508	81312	70224	97393	58118
Flue gas flow rate V_{sp}, nm^3/h	170948	148418	152323	158463	142011	195083	62998

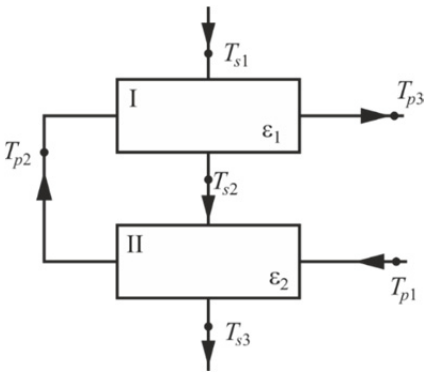

Fig. 3. Air preheater model. T_{s1} – exhaust gas temperature before the air preheater, T_{s2} – exhaust gas temperature halfway up the preheater, T_{s3} – exhaust gas temperature leaving the exchanger, T_{p1} – external air temperature (at the inlet to the preheater), T_{p2} – air temperature in the return duct, T_{p3} – temperature heated air at the outlet of the exchanger.

To determine the flue gas temperature Ts_1 at the air heater inlet, a mathematical model using the ε-NTU method and heat balance equations was developed. For this purpose, the air heater was divided into two single-pass, geometrically identical, cross-flow heat exchangers (Figure 3).

Ambient air temperature T_{p1} and flue gas temperature after heat exchanger T_{s3} were assumed to be known. While other temperatures, including flue gas temperature at the air heater inlet T_{s1} will be determined by solving the system of four equations written for the heat exchanger model depicted in Figure 3.

The equations were as follows [10, 11]

a) heat exchanger I
   - heat balance equation

$$\dot{m}_p c_p\left(T_{p3} - T_{p2}\right) = \dot{m}_s c_{p,s}(T_{s1} - T_{s2}); \tag{1}$$

   - ε-NTU equations for heat exchanger I

$$\varepsilon_1 = \frac{(T_{p3} - T_{p2})}{(T_{s1} - T_{s2})}; \tag{2}$$

and

$$\varepsilon_1 = 1 - exp\left\{\frac{NTU_1^{0.22}}{C^*}[\exp(-C^* \cdot NTU_1^{0.78}] - 1\right\}, \tag{3}$$

where $C^* = \frac{\dot{m}_p c_p}{\dot{m}_s c_{p,s}}$, and $NTU_1 = \frac{U_w A_{w1}}{\dot{m}_p c_p}$

b) heat exchanger II
   - heat balance equation

$$\dot{m}_p c_p\left(T_{p2} - T_{p1}\right) = \dot{m}_s c_{p,s}(T_{s2} - T_{s3}); \tag{4}$$

   - ε-NTU equations for heat exchanger I

$$\varepsilon_2 = \frac{(T_{p2} - T_{p1})}{(T_{s2} - T_{s1})}; \tag{5}$$

and

$$\varepsilon_2 = 1 - exp\left\{\frac{NTU_2^{0.22}}{C^*}[\exp(-C^* \cdot NTU_2^{0.78}] - 1\right\}, \tag{6}$$

where $C^* = \frac{\dot{m}_p c_p}{\dot{m}_s c_{p,s}}$, and $NTU_2 = \frac{U_w A_{w2}}{\dot{m}_p c_p}$

Calculation of the temperature of fluids flowing through the air heater was carried out for the assumed five ambient air temperatures: -20°C, -10°C, 0°C, 10°C and 20°C. Examples of calculation for selected fuel compositions are presented in Table 3.

Table 3. Results of the calculation of the heat transfer coefficient on the flue gas side h_s and air side h_p and the flow velocities of the working medium for the different outside air temperatures T_{p_1} and the composition of the burnt fuel.

Fuel Mix 4						
Air temperature, °C	T_{p1}	-20.0	-10.0	0.0	10.0	20,0
	T_{p2}	135.0	138.6	142.1	145.5	148.9
	T_{p3}	190.6	191.6	192.5	193.6	194.2
Flue gas temperature, °C	T_{s1}	208.3	208.3	208.3	208.3	208.3
	T_{s2}	183.6	184.7	185.9	186,9	188.1
	T_{s3}	115.6	119.5	123.4	127.4	131.4
Actual air volumetric flow rate V_p^r, m^3/h		75 359	78 336	81 312	84 289	87 266
Actual air mass flow rate $\dot{m}_p$, kg/s		28,8	28.8121	28.8086	28.8054	28.8024
Maximum velocity w_{max}, m/s		2.8504	2.9	3.1	3. 2	3.3
Air side heat transfer coefficient h_p, $W/(m^2 \cdot K)$		45.3	46.1	46.8	47.4	48.1
Actual flue gas volumetric flow rate V_s^r, m^3/h		279 282	279 282	279 282	279 282	279 282
Actual flue gas mass flow rate $\dot{m}_s$, kg/s		62.0	62.0	62.0	62.0	62.0
Flue gas velocity w_s, m/s		8.9	8.9	8.9	8.9	8.9
Flue gas side heat transfer coefficient h_s, $W/(m^2 \cdot K)$		36.8	36.8	36.8	36.8	36.8
Overall heat transfer coefficient U_w, $W/(m^2 \cdot K)$		20.99	21.14	21.27	21.40	21.52

To verify the correctness of the determination of the flue gas temperature at the inlet to the APH, it was compared with the available measurements carried out on the boiler by the DCS.

Inlet flue gas temperature T_{s1}, mass flow rates of flue gas $\dot{m}_s$ and air $\dot{m}_p$ together with the assumed outside air temperatures T_{p1} determined for the various compositions of burnt fuel were served as input data for further modelling using computational fluid mechanics (CFD).

4 CFD simulation of air heater operation

The air heater's operating conditions were analysed using computational fluid mechanics (CFD). As boundary condition, the flue gas composition, air and flue gas volumetric flow rates calculated for the selected fuel mixture, the ambient air temperature (T_{p1}) and flue gas temperature (T_{sp2}) at the inlet to the first section of the air preheater (APH) calculated using the developed mathematical model of the two-pass cross-current air preheater (Section 3) were used. A 3D numerical model of the first pass of the heat exchanger was defined based on the technical documentation (Figure 4).

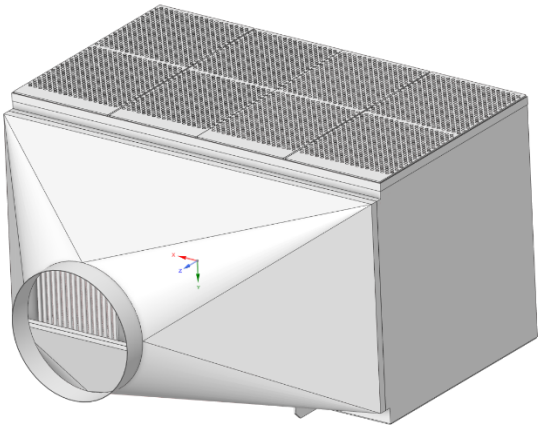

Fig. 4. Numerical model of the first pass of the air preheater (APH).

For the computational model shown in Figure 4, an analysis was carried out to determine the effect of the finite element mesh density on the determined values of the working fluids and metal temperature. In addition, an optimum mesh layout was selected for the coupled thermal-fluid analysis to represent the boundary layer on the air and flue gas side. The study performed for four subdivisions with the following finite element numbers: $4.9 \cdot 10^7$, $6.5 \cdot 10^7$, $8.7 \cdot 10^7$ and $9.9 \cdot 10^7$ show that a subdivision of $6.5 \cdot 10^7$ finite elements starts to play less role on the determined tube inner surface temperature values.

In modelling the operation of the air heater, a computational domain consisting of $8.7 \cdot 10^7$ finite elements was used.

In the next stage of modelling the processes occurring in the air heater, the effect of the length of the external air supply duct on the calculated temperatures of the working media and the speed and direction of the airflow in the exchanger was analysed. Thanks to symmetry, it was possible to carry out tests on a simplified heat exchanger model.

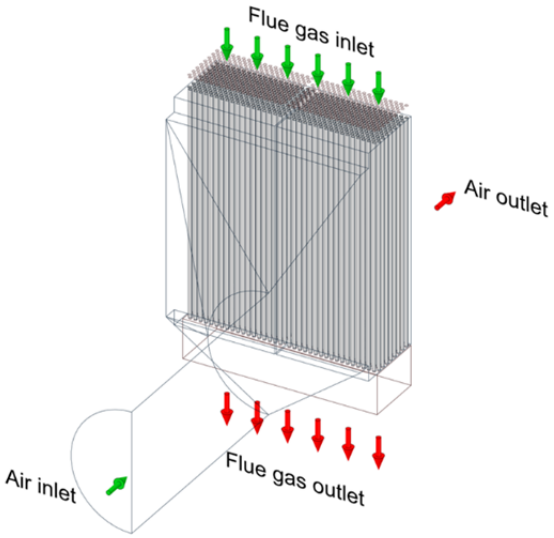

Fig. 5. Scope of the CFD model of the air heater under study (16 rows) with boundary conditions applied.

Evaluation of the results obtained from the initial stage of the air preheater modelling allowed the development of its final numerical model. This model consisted of a section of the external air supply duct with a circular cross-section, a connector to the exchanger, which is the transition between the circular duct and the rectangular cross-section (an abrupt extension of the duct), the first four rows of flue gas tubes, a plate fixing the sieve bottom (Figure 5).

The air preheater model shown in Figure 5 was used to analyse the causes of corrosion of the air preheater and tube failure of the blast furnace gas preheater installed in the third pass of the power steam boiler The calculations were carried out for seven types of fuel being combusted, being mixtures of blast furnace gas, coke oven gas and natural gas with different volume shares and outside air temperatures of -10°C, 0°C and 20°C respectively.

4.1 Results of thermal-fluid modelling of air operating conditions

The results of CFD modelling of the operation of the combustion air heater (APH) will be presented using the example of combustion in a boiler of a mixture of coke and blast furnace gases with volume shares of 3.53% and 96.47%, respectively (Mix 4). The calculated properties of the flue gas and air, such as the volume flux, mass flux, the velocity at which each medium flows, the heat entry coefficients and the heat transfer coefficient are shown in Table 3.

a)

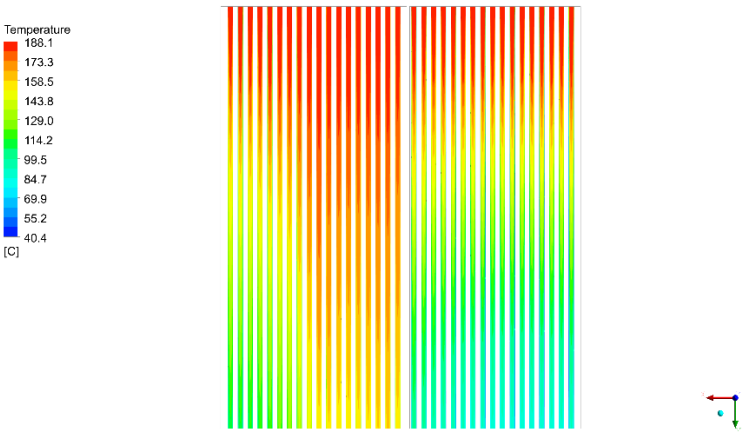

b)

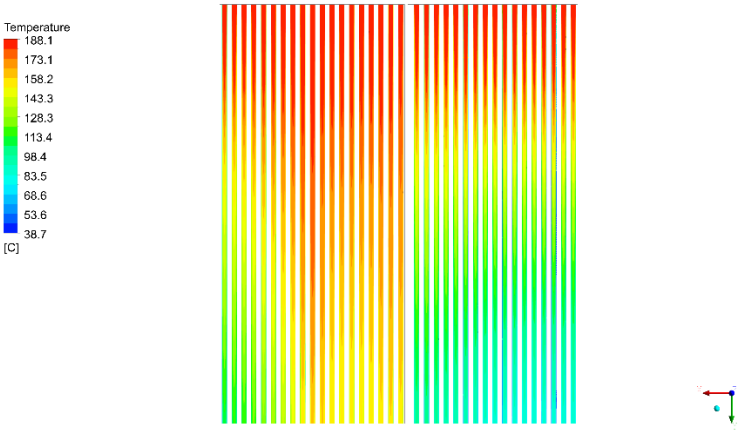

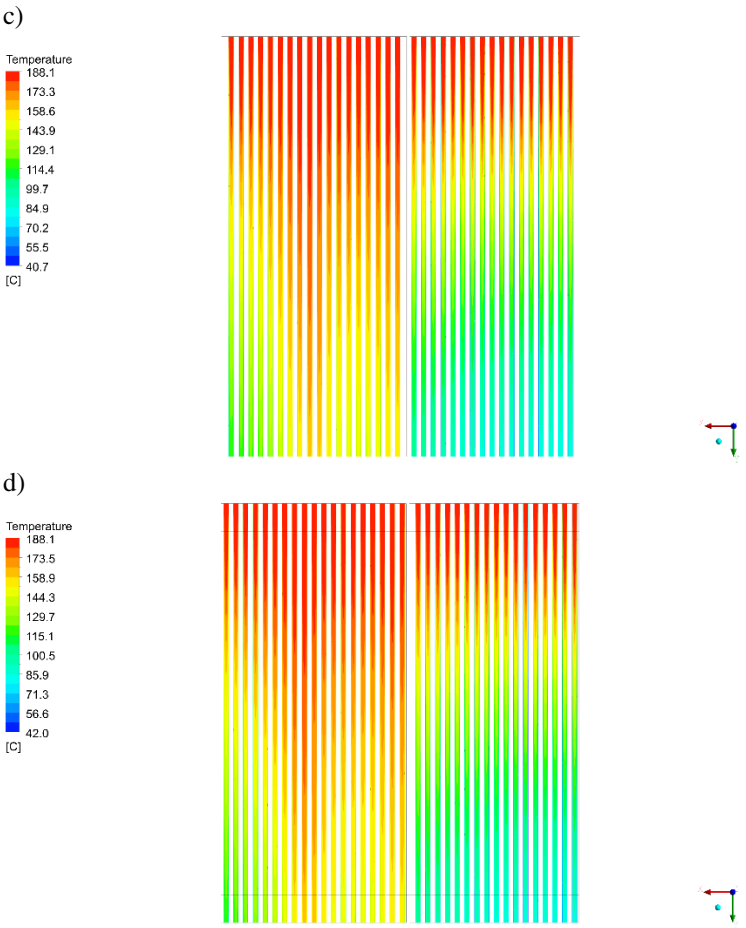

Fig. 6. Determined temperature distributions of the flue gas inside the tubes in the first (a), second (b), third (c) and fourth (d) rows of the air heater tube bundle from the side of the incoming external air at 20°C.

Figures 6a-6d shows the determined temperature distributions of the exhaust gas flowing inside the heat exchanger tubes for an assumed outside air temperature of 20°C. From inspections of Fig. 6a-6d, the zones of the air heater where the heat exchange takes place very intensively can be seen. This results in a significantly lower temperature of the flue gases flowing inside the tubes. The areas of intensive heat transfer are located in the lower part of the heat exchanger, on its right side. The temperature distribution of the flue gases flowing inside the tubes on the left side of the heater model is the opposite. It is notably higher, indicating the very low velocity at which air flows through this area. This situation occurs on each of the four rows of tubes. As shown in the figures above, the flue gas leaving the heat exchanger cools down drastically in the central part of the heat exchanger. The temperature of the flue gas flowing in the first row of the heater tube bundle decreases from 188°C at the inlet to close to 70°C.

To understand the nature of the airflow through the air preheater, the numerical model of the exchanger was extended - the number of combustion tube rows was increased to 40. Aerodynamic calculations were carried out for an external air volume flow rate of 87267 m^3/h and a temperature T_{p1} at the heater inlet of 20ºC (Table 3).

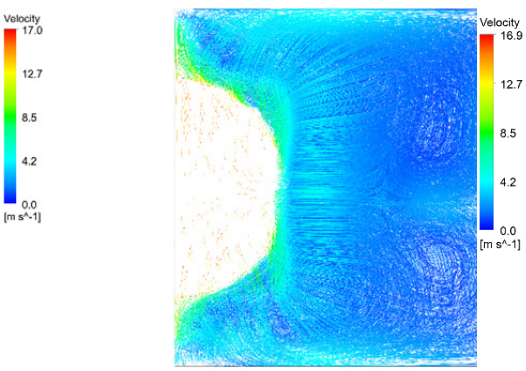

Fig. 7. Current lines of air flowing in the connector between the circular duct and the exchanger (abrupt change zone) - view from the heater side.

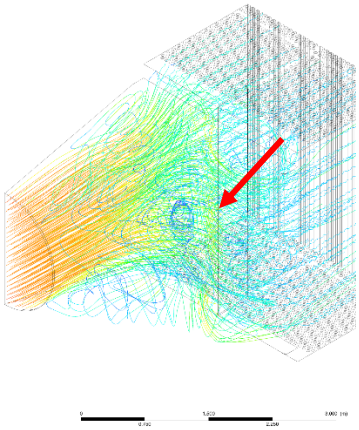

Fig. 8. Air flow current lines in the APH air heater model.

The calculation results are shown in Figure 7 and Figure 8 illustrate the distribution of air velocity in the inlet and connecting duct to the heater. The abrupt change in cross-section, which takes place over a very short distance, results in very high air turbulence in the lateral parts of the connector (left and right of the circular duct fluid outlet), accompanied by backflows. The way in which the air washes over the tubes forming the heating bundles is illustrated by the distribution of air velocities in the heater is shown in Figure 8. In the centre of the exchanger, the air flows with the highest velocity and volume flow. The tube bundle located at the side of the heater model is washed to a small extent. This situation is because the connecting section allowing the cross-sectional change is short, and the plate used to fix the sieve plates (marked in Figure 8 with an arrow) further impedes the airflow by creating, as it were, an extension of the supply channel.

5 Conclusion

The numerical modelling carried out clearly shows that the reason for damage to the air and water heater tubes in the boiler under analysis is too deep cooling of the flue gases. Condensation of water vapour from the flue gases occurs due to the low flue gas temperature and results in the formation of sulphuric acid solution on the tube's inner surface. An additional factor contributing to the excessive cooling of the air heater tubes is its improper design, resulting in air flowing through its central part. This significantly reduces the temperature of the tube walls in the centre of the air heater.

The most important parameter for the dew point temperature is the metal temperature, not the flue gas temperature. If the flue gas temperature is higher than the dew point temperature while the metal tube temperature is lower, condensation of corrosive acid can occur. Low air temperature decreases the metal temperature of the tube and creates favourable conditions for H_2SO_4 condensation.

To be able to operate at low flue gas temperatures and with high efficiency of the boiler and to avoid corrosion at low temperatures, SO_3 should be eliminated from the flue gas when it is still in the furnace chamber because then the dew point temperature will be lowered and no corrosion conditions arise. Corrosion typically occurs during low or variable load boiler operation, at boiler start-ups and periodic planned or unplanned shutdowns, which accelerate the condensation of water vapours.

This work was partially funded by the National Science Centre in Poland within the framework of research project no. 2021/43/B/ST8/01170.

References

1. R. Ebara, F. Tanaka, M. Kawasaki, Sulfuric acid dew point corrosion in waste heat boiler tube for copper smelting furnace, Eng. Fail. Anal. **33** (2013), pp. 29–36. https://doi.org/10.1016/j.engfailanal.2013.04.007
2. Y. Kawahara, High temperature corrosion mechanisms and alloying elements for materials used in waste incineration environment, Corros. Sci. **44** (2002), pp. 223-245. https://doi.org/10.1016/S0010-938X(01)00058-0
3. J.M. Blanco, F. Pena, Increase in the boiler's performance in terms of the acid dew point temperature: Environmental advantages of replacing fuels, Appl. Therm. Eng. **28**, 7 (2008), pp. 777-784. https://doi.org/10.1016/j.applthermaleng.2007.06.024
4. S. Kumar, P. Tadge, A. Mondal, N Hussain, S. Ray, A. Saha, Boiler tube failures in thermal power plant: Two case studies, Mater. Today-Proc., **66(9)** (2022) pp. 3847-3852. https://doi.org/10.1016/j.matpr.2022.06.254
5. A. Marx, D. Hülsbruch, A. Müller, B. Epple, F. Ewert, J. Peitan, Online corrosion monitoring in industrial boilers, Therm. Sci. Eng. Prog. **43** (2023) 102009. https://doi.org/10.1016/j.tsep.2023.102009
6. K. Węglarz, D. Taler, J. Taler, M. Marcinkowski, General numerical method for hydraulic and thermal modelling of the steam superheaters, Energy **291** (2024), 130371. https://doi.org/10.1016/j.energy.2024.130371
7. L. Yin, H. Zhou, Modal decomposition integrated model for ultra-supercritical coal-fired power plant reheater tube temperature multi-step prediction, Energy **292** (2024) 130521. https://doi.org/10.1016/j.energy.2024.130521
8. N. Modliński, K. Szczepanek, D. Nabagło, P. Madejski, Z. Modliński, Mathematical procedure for predicting tube metal temperature in the second stage reheater of the operating flexibly steam boiler, Appl. Therm. Eng. **146** (2019) pp. 854-865. https://doi.org/10.1016/j.applthermaleng.2018.10.063
9. S. Chantasiriwan, Optimum installation of economizer, air heater, and flue gas dryer in biomass boiler, Comput. Chem. Eng., **150** (2021) 107328. https://doi.org/10.1016/j.compchemeng.2021.107328
10. D. Taler, Numerical Modelling and Experimental Testing of Heat Exchangers, Springer, Cham (2018)
11. ANSYS, Inc. ANSYS Fluent User’s Guide, Release 20.2. (2016)